University of Nebraska - Lincoln
DigitalCommons@University of Nebraska - Lincoln

Faculty Publications from the Department of Engineering Mechanics

Mechanical & Materials Engineering, Department of

1-1-2009

Convergence, adaptive refinement, and scaling in 1D peridynamics

Florin Bobaru Ph.D.
University of Nebraska at Lincoln, fbobaru2@unl.edu

Mijia Yabg Ph.D.
University of Nebraska at Lincoln

Leonardo F. Alves M.S.
University of Nebraska at Lincoln

Stewart A. Silling Ph.D.
Sandia National Laboratories

Ebrahim Askari Ph.D.
Boeing Co., Bellevue, WA

See next page for additional authors

Follow this and additional works at: http://digitalcommons.unl.edu/engineeringmechanicsfacpub

Part of the Applied Mechanics Commons, Computational Engineering Commons, Engineering Mechanics Commons, and the Mechanics of Materials Commons

Bobaru, Florin Ph.D.; Yabg, Mijia Ph.D.; Alves, Leonardo F. M.S.; Silling, Stewart A. Ph.D.; Askari, Ebrahim Ph.D.; and Xu, Jifeng Ph.D., "Convergence, adaptive refinement, and scaling in 1D peridynamics" (2009). *Faculty Publications from the Department of Engineering Mechanics.* Paper 68.
http://digitalcommons.unl.edu/engineeringmechanicsfacpub/68

This Article is brought to you for free and open access by the Mechanical & Materials Engineering, Department of at DigitalCommons@University of Nebraska - Lincoln. It has been accepted for inclusion in Faculty Publications from the Department of Engineering Mechanics by an authorized administrator of DigitalCommons@University of Nebraska - Lincoln.

Authors
Florin Bobaru Ph.D., Mijia Yabg Ph.D., Leonardo F. Alves M.S., Stewart A. Silling Ph.D., Ebrahim Askari Ph.D., and Jifeng Xu Ph.D.

This article is available at DigitalCommons@University of Nebraska - Lincoln: http://digitalcommons.unl.edu/engineeringmechanicsfacpub/68

INTERNATIONAL JOURNAL FOR NUMERICAL METHODS IN ENGINEERING
Int. J. Numer. Meth. Engng 2009; **77**:852–877
Published online 26 August 2008 in Wiley InterScience (www.interscience.wiley.com). DOI: 10.1002/nme.2439

Convergence, adaptive refinement, and scaling in 1D peridynamics

Florin Bobaru[1,*,†,‡], Mijia Yang[1,4], Leonardo Frota Alves[1], Stewart A. Silling[2], Ebrahim Askari[3] and Jifeng Xu[3]

[1]*Department of Engineering Mechanics, University of Nebraska-Lincoln, Lincoln, NE, U.S.A.*
[2]*Multiscale Dynamic Material Modeling Department, Sandia National Laboratories, Albuquerque, NM, U.S.A.*
[3]*Boeing Co., Bellevue, WA, U.S.A.*
[4]*Department of Civil and Environmental Engineering, University of Texas - San Antonio, San Antonio, TX, U.S.A.*

SUMMARY

We introduce here adaptive refinement algorithms for the non-local method peridynamics, which was proposed in (*J. Mech. Phys. Solids* 2000; **48**:175–209) as a reformulation of classical elasticity for discontinuities and long-range forces. We use scaling of the micromodulus and horizon and discuss the particular features of adaptivity in peridynamics for which multiscale modeling and grid refinement are closely connected. We discuss three types of numerical convergence for peridynamics and obtain uniform convergence to the classical solutions of static and dynamic elasticity problems in 1D in the limit of the horizon going to zero. Continuous micromoduli lead to optimal rates of convergence independent of the grid used, while discontinuous micromoduli produce optimal rates of convergence only for uniform grids. Examples for static and dynamic elasticity problems in 1D are shown. The relative error for the static and dynamic solutions obtained using adaptive refinement are significantly lower than those obtained using uniform refinement, for the same number of nodes. Copyright © 2008 John Wiley & Sons, Ltd.

Received 21 December 2007; Revised 3 June 2008; Accepted 8 July 2008

KEY WORDS: peridynamics; non-local methods; adaptive refinement; convergence; multiscale modeling

*Correspondence to: Florin Bobaru, Department of Engineering Mechanics, University of Nebraska-Lincoln, Lincoln, NE, U.S.A.
†E-mail: fbobaru2@unl.edu
‡Associate Professor.

Contract/grant sponsor: Boeing Co.; contract/grant number: DE-AC04-94AL85000
Contract/grant sponsor: Computer Science Research Foundation and Computer Science Research Institute at Sandia National Laboratories

Copyright © 2008 John Wiley & Sons, Ltd.

This article is a U.S. government work, and is not subject to copyright in the United States.

1. INTRODUCTION

1.1. Literature review

Adaptive grid refinement techniques have been introduced in numerical simulations in order to gain both accuracy and efficiency. Capturing stress and strain concentrations near cracks, for example, requires dense computational grids. Adaptive methods permit reduction of grid density away from steep gradients thus rendering the computational problems tractable. Error estimators are required to determine where grid refinement is necessary. Adaptive methods for finite element methods (FEM) have been studied for the past three decades (see, e.g. [1, 2]). Automatic and goal-oriented h, p, and hp-adaptive strategies for FEM have been introduced and discussed in [3–6].

While many applications of adaptive refinement methods in FEM have been developed for static problems, adaptivity for dynamic problems has also been studied (e.g. [7–10]). In 1D time-dependent problems, several additional issues have to be dealt with, such as (see [7, 8]) spurious reflections of waves over non-uniform grids. A local error estimator and an adaptive time-stepping procedure for dynamic analysis are proposed in [9]. Dispersion effects due to FE spatial discretization are also discussed in [11]. Adaptive finite element approximations for the acoustic wave equation using a global duality argument and Galerkin orthogonality are presented in [12], while in [10] automatic energy conserving space–time refinement techniques for dynamic FEM are shown. The method presented in [10] performs automatic refining and coarsening for the wave propagation problem in 1D. Adaptive discontinuous Galerkin FEM for dynamic problems are developed in [13].

In multiple dimensions, the grid generation for adaptive refinement becomes more complex and special algorithms have been proposed. One of the simplest is using quad tree structures (in 2D) and has been used in the context of finite volume method in [14–16], for FEM in [17], and with the meshfree element-free Galerkin method [18], where level-1 quad-tree structures are employed even though this is not explicitly mentioned in the paper. The level-1 (or 1-irregular) grid refinement has been originally introduced in [1].

In the present study we introduce algorithms and show convergence results regarding adaptive grid refinement algorithms for static and dynamic elasticity problems in 1D for a non-local method, the peridynamic formulation. Non-local methods are necessary in modeling of localization phenomena, such as fracture, damage, shear bands, for reasons described in detail in the review paper [19]. Adaptive refinement for other non-local methods applied to damage problems and discretized using the finite element method has appeared in, for example, [20–23]. These methods cannot be directly applied to peridynamics because the peridynamic formulation, first introduced in [24], is different from other non-local methods. We discuss this topic briefly below.

1.2. Overview of peridynamics

The peridynamic method, introduced in [24], is a non-local formulation of continuum mechanics in which each material point is connected (via peridynamic bonds) with nodes in a certain region around it and not only with its nearest neighbors. The method is particularly well suited for dealing with cracks and damage in solid mechanics (see [25, 26]) especially in situations where the crack path, for example, is not known in advance. The method also allows for easy introduction of long-range forces, such as van der Waals interactions and examples of deformation and damage at the nanoscale are treated in [26, 27]. In fact, all forces in the peridynamic formulation are long-range. Other non-local methods have been proposed over the years: see, e.g. [28–33]. For a recent review

Copyright © 2008 John Wiley & Sons, Ltd.

DOI: 10.1002/nme

of other non-local methods, we refer the reader to [19]. Peridynamics differs from other integral non-local methods in at least two crucial aspects: (1) spatial derivatives are eliminated while other methods average infinitesimal stresses over a certain area and (2) the way damage and fracture are introduced in the method (see [26]).

A description of a meshfree numerical implementation for the peridynamic formulation is given in [25], where bond failure is related to the classical energy release rate in brittle fracture. The method is used in [26] to simulate the tearing of non-linear membranes and failure of nanofiber networks (see also [27]). Spontaneous fracture initiation and dynamic propagation are captured and membrane wrinkling and the influence of Van der Waals forces in nanofiber networks are discussed.

Classical continuum mechanics has been applied to explain the behavior of structural bodies which remain continuous as they deform under external loads. However, the effectiveness of computational methods based on classical continuum mechanics, such as finite elements, in modeling material failure has lagged far behind their capabilities in traditional stress analysis. This difficulty arises because these methods solve the classical equations of continuum mechanics, which are a set of partial differential equations. These equations cannot be applied directly across discontinuities resulted from material damage and failure, as the required partial derivatives do not exist there. This mathematical breakdown results in great difficulties in attempting to model material failure directly and leads to special techniques in fracture mechanics to treat discontinuities, such as cracks, as a pathological situation. These limitations become particularly inconvenient in the case of composite materials because it is very difficult to track individual defects, which grow in constituent materials, along interfaces, and between different layers, and moreover, interact with each other.

The peridynamic theory is a mathematical framework for continuum mechanics that does not involve spatial derivatives of the displacement field [24]. It reformulates the basic equations of motion in such a form that the internal forces are evaluated through an integral formulation that does not require the evaluation of a stress tensor field or its spatial derivatives [34]. The peridynamic theory does not suffer from the inapplicability when discontinuities are present and offers a unique capability to predict material failure. In the peridynamic theory, the emergence and growth of discontinuous areas, such as fractures or cracks, are treated as just another form of deformation, rather than as pathological cases. Internal forces within a continuous body are expressed through interactions, called bonds, between pairs of particles. Damage is part of the constitutive model, and the material response is determined at the bond level. Defects grow and propagate when and where it is energetically favorable for them to do so. There is no need for an externally supplied law or the special techniques of fracture mechanics, as material defects can evolve in complex patterns not known in advance. Therefore, the peridynamic approach offers the potential to simulate complex patterns of mutually interacting material defects in great generality.

The numerical model of peridynamic theory has been successfully applied to damage analysis of metallic structures and nano-scale structures [25–27]. Recently, its application was extended to damage and failure analysis of composite materials. In [35], the peridynamic method has been applied to predict the failure modes of large-notched composite panels with different lay-ups under tension loads and the delamination area in composites laminates impacted with different energy levels ranging from 22.6 to 135.6 J. The results have reproduced the experimentally observed dependence of failure modes on the relative percentage of fibers in different orientations. The delamination areas from peridynamic simulations also agree well with the experimental data. In [36], the failure modes and residual strengths of cruciform composite plates under more realistic

Copyright © 2008 John Wiley & Sons, Ltd.

DOI: 10.1002/nme

biaxial loads are modeled using the peridynamic theory. The simulation results agree well with the experimental ones. In [37], the effects of void content on stiffness and strength of composite structures are studied by a peridynamic analysis and static indentation test. The simulated damage areas are in good agreement with the experimental damage measurements.

1.3. Our contributions

In this paper we introduce a method for adaptive grid refinement for the non-local peridynamic method. As with any new method, the relationship between peridynamics and classical (local) elasticity needs to be explored. We discuss convergence of the peridynamic solution to that of the classical, local, elasticity solution for two sample static and dynamic problems.

We introduce three different types of convergence that one can use to compare the numerical peridynamic solutions with the classical elasticity solutions for regular problems (without discontinuities). We show that the particular shape and smoothness of the micromodulus function (see below for definition of micromodulus function) have an influence on the rate of convergence of the adaptive schemes. Since classical elasticity has no length-scale, the comparison with the peridynamics results has to be done by taking the peridynamic horizon to zero.

The examples we give from static and dynamic analyses in 1D show that the adaptive peridynamic solution achieves the same or very similar rates of convergence as uniform refinement, which is expected for problems where strain concentrations do not appear. The relative error with adaptive refinement is significantly lower than with uniform refinement for the same number of nodes. The advantage of adaptive refinement is critical in problems where localized areas present strain and stress concentrations, like the tip of cracks. Our current efforts are directed at extending the ideas presented here to problems involving crack propagation in 2D and 3D. It is in this types of problems that peridynamics has shown its greatest advantages when compared with classical methods. The present development is a first step in constructing multiscale algorithms for peridynamics.

The paper is organized as follows: in the next section we review the peridynamic formulation for a 1D elastic bar and give several examples of possible micromodulus functions. In Section 3 we introduce three types of convergence that are relevant when trying to compare the peridynamic solutions with those of classical elasticity, and we analyze the behavior of the numerical peridynamic approximation for the 1D bar under self-equilibrated loads. In Section 4 we introduce the new scheme for adaptive refinement in peridynamics, which involves scaling the micromodulus function with the horizon, as well as a new 'visibility criterion'. Examples and results on rates of convergence to the classical solutions are shown in Section 5 for an elasto-static problem and in Section 6 for an elastic wave propagation problem. We present conclusion in the final Section 7.

2. PERIDYNAMIC FORMULATION FOR A SELF-EQUILIBRATED 1D BAR

In this section, we first review the peridynamic formulation in 1D. We then present the peridynamic analytical solution for the specific problem of a 1D bar loaded by two opposing point forces, also discussed in [38]. We comment on the numerical discretization of this problem for the case of constant micromodulus.

The peridynamics equations of motion are given by [24]

$$\rho\ddot{\mathbf{u}}(\mathbf{x},t)=\int_H \mathbf{f}(\mathbf{u}(\widehat{\mathbf{x}},t)-\mathbf{u}(\mathbf{x},t),\widehat{\mathbf{x}}-\mathbf{x})\,\mathrm{d}V_{\widehat{\mathbf{x}}}+\mathbf{b}(\mathbf{x},t) \tag{1}$$

Copyright © 2008 John Wiley & Sons, Ltd.

DOI: 10.1002/nme

while for statics we have,

$$\int_H \mathbf{f}(\mathbf{u}(\widehat{\mathbf{x}},t)-\mathbf{u}(\mathbf{x},t),\widehat{\mathbf{x}}-\mathbf{x})\,\mathrm{d}V_{\widehat{\mathbf{x}}}+\mathbf{b}(\mathbf{x},t)=0 \tag{2}$$

In the above, $\mathbf{f}$ is the pairwise force in the peridynamic bond that connects particle $\widehat{\mathbf{x}}$ to $\mathbf{x}$, and where $\boldsymbol{\xi}=\widehat{\mathbf{x}}-\mathbf{x}$ is the relative position in the reference configuration and $\boldsymbol{\eta}=\widehat{\mathbf{u}}-\mathbf{u}$ is the relative displacement. $\rho(\mathbf{x},t)$ is the density while $\mathbf{b}(\mathbf{x},t)$ is the body force. The integrals are defined over a region H called the 'horizon', which is the support of the pairwise force function around point $\mathbf{x}$.

A microelastic material [24] is defined as one for which the pairwise force derives from a potential w:

$$\mathbf{f}(\boldsymbol{\eta},\boldsymbol{\xi})=\frac{\partial w(\boldsymbol{\eta},\boldsymbol{\xi})}{\partial \boldsymbol{\eta}} \tag{3}$$

A *linear microelastic potential* is obtained if we take

$$w(\boldsymbol{\eta},\boldsymbol{\xi})=\frac{c(\|\boldsymbol{\xi}\|)s^2\|\boldsymbol{\xi}\|}{2} \tag{4}$$

where

$$s=\frac{\|\boldsymbol{\xi}+\boldsymbol{\eta}\|-\|\boldsymbol{\xi}\|}{\|\boldsymbol{\xi}\|} \tag{5}$$

is the *bond-strain*. Note that this is not the usual infinitesimal strain, but rather the *relative elongation* of a bond. The function $c(\|\boldsymbol{\xi}\|)$ has the meaning of the bond elastic stiffness. For such a material, the magnitude of the force in a bond varies linearly with its bond-strain. Indeed,

$$\mathbf{f}(\boldsymbol{\eta},\boldsymbol{\xi})=\nabla_{\boldsymbol{\eta}}w(\boldsymbol{\eta},\boldsymbol{\xi})=cs\|\boldsymbol{\xi}\|\nabla_{\boldsymbol{\eta}}s=cs\nabla_{\boldsymbol{\eta}}\|\boldsymbol{\xi}+\boldsymbol{\eta}\|=c(\|\boldsymbol{\xi}\|)s\mathbf{e} \tag{6}$$

where $\mathbf{e}$ is the unit vector along the direction of the relative position vector in the current configuration, $\boldsymbol{\xi}+\boldsymbol{\eta}$:

$$\frac{\partial\|\boldsymbol{\xi}+\boldsymbol{\eta}\|}{\partial\boldsymbol{\eta}}=\frac{1}{\|\boldsymbol{\xi}+\boldsymbol{\eta}\|}(\xi_1+\eta_1,\xi_2+\eta_2,\xi_3+\eta_3)=\mathbf{e} \tag{7}$$

For a 1D bar the micropotential of the material is given by

$$w=\frac{c(|\xi|)s^2|\xi|}{2} \tag{8}$$

and the corresponding pairwise force has the following magnitude:

$$f=c(|\xi|)s \tag{9}$$

The elastic energy density for the 1D bar of constant cross-section area A, can be calculated as

$$W=\frac{1}{2}\int_H w(\eta,\xi)\,\mathrm{d}V_\xi=\frac{A}{2}\int_{-\delta}^{\delta}w(\eta,\xi)\,\mathrm{d}\xi=\frac{A}{4}\int_{-\delta}^{\delta}c(|\xi|)s^2|\xi|\,\mathrm{d}\xi \tag{10}$$

where δ is the horizon 'radius'. Note that W is the strain elastic energy per unit volume at a point within the body.

Copyright © 2008 John Wiley & Sons, Ltd.

DOI: 10.1002/nme

The micromodulus function is required to satisfy certain conditions of regularity (see [38]). The types of allowable functions, however, are quite large. We note that the smoothing regularization of the micromodulus function given in [39] is not necessary. We give examples of continuous and discontinuous micromodulus functions and describe the numerical sensitivity and behavior of the solution to these functions.

For homogeneous deformations, the relation between a classical linear elastic material and the parameters for a micromodulus constant over its horizon is given in [25]. Other forms for the micromodulus are possible, and the specific shape should, in principle, affect only deformations at the scale of the horizon. We shall see, however, that in adaptive grid refinement, the smoothness of the micromodulus function plays a role in the rate of convergence obtained. We next provide the derivations for relating the 'constant', 'triangular', and the 'inverted triangular' micromoduli to a classical linear elastic material.

2.1. Examples of micromodulus functions

The constant micromodulus is used here to define a microelastic material given by

$$f(x,\hat{x},u,\hat{u})=c(|\xi|)s=\begin{cases} c_0 s & \text{if } |\xi|\leqslant\delta \\ 0 & \text{if } |\xi|>\delta \end{cases} \tag{11}$$

where c_0 is the peridynamic bond stiffness that is independent of bond length (see Figure 1(a)). Note that the constant micromodulus has jump discontinuities at $\xi=\pm\delta$. We assume a homogeneous deformation, thus the strain in any bond does not depend on location: $s(x)=s=\text{const}$. The micropotential of the material is thus given by

$$w=\tfrac{1}{2}c_0 s^2|\xi| \tag{12}$$

and its elastic energy density can be calculated as,

$$W=\frac{A}{4}\int_{-\delta}^{\delta} c_0 s^2|\xi|\,\mathrm{d}\xi=\frac{Ac_0 s^2\delta^2}{4} \tag{13}$$

The elastic energy density of classical theory is $W_0=Es^2/2$, where E is the elastic modulus. Setting the energy in Equation (13) equal to the elastic energy density of the classical theory and

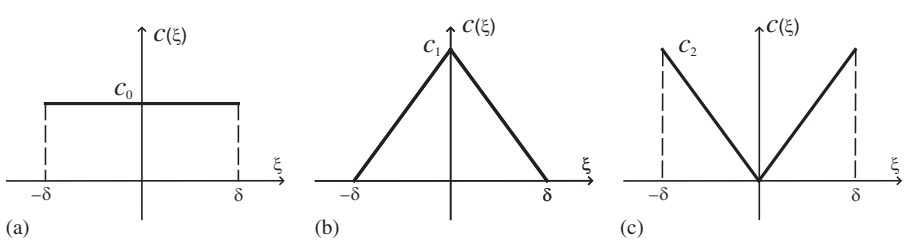

Figure 1. Examples of micromodulus functions: discontinuous: constant in (a); and inverted triangular in (c) and continuous piecewise linear: triangular in (b).

Copyright © 2008 John Wiley & Sons, Ltd.

DOI: 10.1002/nme

solving for c_0 gives

$$c_0 = \frac{2E}{\delta^2 A} \tag{14}$$

Thus,

$$c(|\xi|) = \begin{cases} \dfrac{2E}{\delta^2 A}, & |\xi| \leqslant \delta \\ 0, & |\xi| > \delta \end{cases} \tag{15}$$

A continuous micromodulus function with a triangular profile (see Figure 1(b)) is given by

$$c(|\xi|) = \begin{cases} c_1 \left(1 - \dfrac{|\xi|}{\delta}\right) & \text{if } |\xi| \leqslant \delta \\ 0 & \text{if } |\xi| > \delta \end{cases} \tag{16}$$

The elastic strain energy in this case is

$$W = \frac{A}{4} \int_{-\delta}^{\delta} c(|\xi|) s^2 |\xi| \, \mathrm{d}\xi = \frac{A c_1 s^2 \delta^2}{12} \tag{17}$$

which results in a value

$$c_1 = \frac{6E}{\delta^2 A} \tag{18}$$

Smoother functions can be used but this will not be pursued further here.

A more 'exotic' micromodulus function is given by the inverted triangular function shown in Figure 1(c) (this was used also in [38]; see comments below). In this case, the bonds connecting nodes that are near the source node are 'softer' than bonds connecting the source node with nodes that are farther away. At the edge of the horizon a sudden drop to zero takes place. This inverted triangular micromodulus functions is defined as follows:

$$c(|\xi|) = \begin{cases} c_2 \dfrac{|\xi|}{\delta} & \text{if } |\xi| \leqslant \delta \\ 0 & \text{if } |\xi| > \delta \end{cases} \tag{19}$$

The elastic strain energy in this case is

$$W = \frac{A}{4} \int_{-\delta}^{\delta} c(|\xi|) s^2 |\xi| \, \mathrm{d}\xi = \frac{A c_2 s^2 \delta^2}{6} \tag{20}$$

To compute the constant c_2, we equate this elastic energy density with that computed classically, resulting in

$$c_2 = \frac{3E}{A\delta^2} \tag{21}$$

Please note that in this case, the function $C(|\xi|)$ in [38] becomes a constant. The meaning of the function $C(|\xi|)$ is the *spring stiffness*, whereas the function $c(|\xi|)$ used in the present work has

Copyright © 2008 John Wiley & Sons, Ltd.

DOI: 10.1002/nme

the meaning of *elastic stiffness*. Indeed

$$C(|\xi|)=\frac{c(|\xi|)}{|\xi|}=\frac{3E}{A\delta^3}=C \tag{22}$$

The influence of the specific form of the micromodulus on computations will be studied in the following sections.

2.2. Analytical solution of 1D equilibrated peridynamic bar under two concentrated forces

Here we follow [38] and give the analytical solution for the problem of the self-equilibrated 1D bar. We will use this solution to compare with our numerical results.

An 1D bar of infinite length and cross-section area $A=1$ is loaded by a pair of self-equilibrated concentrated forces, of unit magnitude, acting at the points $x=\pm a$, where a is the location of right applied load. In the classical setting, the displacement $u(x)$ along the bar is given by

$$u(x)=\begin{cases}-a/E, & x<-a\\ x/E, & |x|\leqslant a\\ a/E, & x>a\end{cases} \tag{23}$$

Following [38] and using $b(x)=D(x-a)-D(x+a)$, with D being the Dirac-delta distribution, the exact peridynamic solution for the displacement far away from a and $-a$ can be written as

$$u_\infty=\frac{1}{2E}\int_{-\infty}^{\infty}xb(x)\,\mathrm{d}x=\frac{1}{2E}\int_{-\infty}^{\infty}x[D(x-a)-D(x+a)]\,\mathrm{d}x=\frac{a}{E} \tag{24}$$

Note that the micromodulus $C(\xi)$ in [38] is connected to the micromodulus defined here by $C(\xi)=c(|\xi|)/|\xi|$. The micromodulus $c(|\xi|)=c(|\hat{x}-x|)$ used here has the meaning of the elastic stiffness of the bond between x and $\hat{x}$.

In the limit of the horizon $\delta\to 0$, it can be shown [38] that the peridynamic solution converges to the classical elasticity solution (23) almost everywhere. At the locations where the concentrated loads are applied, the peridynamic displacement matches the smoothness of the load, that is it is also singular.

2.3. Numerical solution of 1D peridynamic bar under two concentrated forces

Given a node distribution $x_i, i=1,2,\ldots,N$ over the length of a bar which is much longer than the distance between a and $-a$, we discretize Equation (2) at particle x_i using the composite midpoint integration method,

$$\sum_p c(|x_p-x_i|)\frac{(u_p-u_i)}{|x_p-x_i|}V_{ip}+b_i=0 \tag{25}$$

where $c(|x_p-x_i|)$ is the micromodulus function depending on the different material models used and V_{ip} is the portion of node p 'volume' covered by the horizon of node i. Rewriting the above equations in matrix-vector form,

$$\mathbf{A}\bar{\mathbf{u}}=\bar{\mathbf{b}} \tag{26}$$

one can solve for the nodal displacements in vector $\bar{\mathbf{u}}$ given the vector $\bar{\mathbf{b}}$ corresponding to the applied concentrated load $b(x)=D(x-a)-D(x+a)$.

Copyright © 2008 John Wiley & Sons, Ltd.

DOI: 10.1002/nme

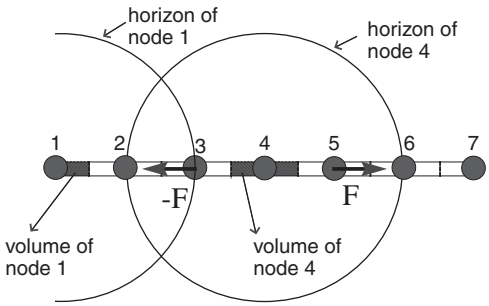

Figure 2. The peridynamic discrete form of a finite length 1D bar under self-equilibrated loads.

For the particular case when we use seven nodes to discretize the bar, the horizon δ equals $2\Delta x$ (so that the horizons for nodes away from the ends cover exactly five nodes—see Figure 2), $E=1$, $b_3=-1$, $b_5=1$, and for case of constant micromodulus function $c_0=2E/\delta^2 A$, the above system reads:

$$
\begin{aligned}
-1.25u_1+u_2+0.25u_3&=0\\
0.5u_1-1.75u_2+u_3+0.25u_4&=0\\
0.25u_1+u_2-2.5u_3+u_4+0.25u_5&=2\\
0.25u_2+u_3-2.5u_4+u_5+0.25u_6&=0\\
0.25u_3+u_4-2.5u_5+u_6+0.25u_7&=-2\\
0.25u_4+u_5-1.75u_6+0.5u_7&=0\\
0.25u_5+u_6-1.25u_7&=0
\end{aligned}
$$

The condition number (in vector norm-2: $\|\mathbf{u}\|_2=\sqrt{\sum_i u_i^2}$) of the matrix $\mathbf{A}$ is 2.8×10^4. This relatively large condition number decreases fast with increasing the number of discretization nodes and decreasing horizon. For the corresponding triangular micromodulus, and the same discretization as above, the condition decreases to 0.7×10^4, while for the 'inverted triangular' micromodulus the condition number blows up in norm-2 (it is 10^{17} in norm-∞ and 10^{18} in norm-1: $\|\mathbf{u}\|_\infty=\max_i |u_i|$, $\|\mathbf{u}\|_1=\sum_i |u_i|$). Notice that the 'exotic' inverted triangular is an acceptable one from the point of view of stability (see [38]). It may appear that the ill-conditioning issue that occurs with the use of a concave micromodulus function prevents computing the numerical solution to the static problem. With the dynamic relaxation method, for example, we avoid this problem since no matrix is formed (see, e.g. [40]) and the correct static solution is obtained even with the inverted triangular micromodulus after a sequence of 'relaxed' dynamic solutions (see, e.g. [41]).

3. CONVERGENCE IN PERIDYNAMICS AND COMPARISONS WITH THE CLASSICAL ELASTICITY SOLUTIONS

Convergence of numerical approximations of the peridynamic equations differs from traditional convergence in the FEM or the FVM. The peridynamic model is non-local and contains a

Copyright © 2008 John Wiley & Sons, Ltd.

DOI: 10.1002/nme

length-scale determined by the horizon δ. Since the classical equations of elasticity have no intrinsic length-scale (or the length-scale is zero) it makes sense to consider here the type of convergence in which the peridynamic horizon goes to zero.

In some problems, particularly at the nanoscale, the horizon is determined by the physics of interactions between particles. Considering values below the atomic interaction for the horizon would not make sense. Notice, however, that at the macroscale level, the horizon may be chosen according to convenience, since for any value of δ, the parameters in the peridynamic material model, such as the micromodulus c, can be chosen to match the measured material parameters, such as the material Young's modulus. The match between measurable material parameters (e.g. elastic modulus) and the peridynamic parameters is 'imposed' for the case of homogeneous deformations (see Equations (14), (18), (21)). In the examples in this section and in Sections 5 and 6, the deformation is not homogeneous. The convergence of the peridynamic solution to the classical one, however, still holds.[§]

To allow large variations in grid spacing within a discretized region, which is useful in practical computations, it is helpful to allow δ to vary with position. Such variability in δ motivates the following discussion on the convergence of the peridynamic equations while both δ and the grid spacing are varied. For further discussion on the horizon's influence, please see [41–43].

3.1. Numerical convergence of 1D peridynamic bar compared with classical local solutions

Here we discuss the numerical convergence for the 1D peridynamic bar problem introduced above. We restrain our discussion to the convergence of the numerical integration for the spatial variable. Time discretization for the dynamic equations will also introduce relative error into the numerical approximation and we discuss this in Section 6.

Considering a set of discretization nodes equally spaced with a spacing Δx so that the region $[x-\delta, x+\delta]$ covers $2m+1$ nodes, and applying the composite midpoint rule for approximating the domain integral in Equations (1) or (2), we can define three types of convergence in peridynamics:

- The (δm)-convergence: $\delta \searrow 0$ and m increases with decreasing δ, with m increasing faster than δ decreases. In this case we will see that the numerical peridynamic approximation converges to the analytical peridynamic solution and converges uniformly to the local classical solution, almost everywhere.[¶]
- The m-convergence: δ is fixed and $m \to \infty$. The numerical peridynamic approximation converges to the exact non-local peridynamic solution for the given δ.
- The δ-convergence: $\delta \to 0$ and m is fixed or increases with decreasing δ but at a slower rate. In this case the numerical peridynamic approximation converges to an approximation of the classical solution, almost everywhere. The larger m is, the closer this approximation becomes. The convergence is not guaranteed to be uniform.

Note that since the horizon δ is required to cover more than its own node, the discretization size has to decrease when δ decreases. Thus, in the limiting process of δ going to zero, m (the ratio between the horizon and the 'volume' of a node) cannot decrease to one. Our discussion

[§]At points where the boundary conditions and the loadings are regular.
[¶]Except, eventually, over a set of measure zero.

Copyright © 2008 John Wiley & Sons, Ltd.

DOI: 10.1002/nme

below and the numerical examples will demonstrate that, in fact, m needs to increase faster than δ decreases in order to achieve uniform convergence.

A detailed discussion on the performance of different quadrature schemes for the peridynamic equations is given in [44].

3.2. Example of behavior of the numerical approximation for a singular solution

The numerical approximation for the 1D peridynamic bar under two concentrated forces is analyzed here for the case of a discontinuous micromodulus (the inverted triangle, which corresponds to the constant C in [38]). The analytical peridynamic solution tends to the classical solution, in the limit of the horizon going to zero, everywhere except at the points of application of the point-loads. At these points, the analytic peridynamic displacement has the same Dirac δ-function behavior as the loading (see [38]). We investigate the various types of convergence of the numerical approximation of the peridynamic solution. We note that the jump discontinuities in the displacement away from the loading points are eliminated with the use of a continuous micromodulus function, such as the triangular one introduced before. We will see later that the continuity (smoothness) of the micromodulus function has consequences on the rate of convergence in adaptive refinement.

For the inverted triangle micromodulus, as we saw in Equation (22), for a bar with unit cross-sectional area, $C(|\xi|)$ is defined as:

$$C=\begin{cases}3E/\delta^3, & |\xi|\leqslant\delta\\ 0, & |\xi|>\delta\end{cases} \tag{27}$$

The inverted triangle micromodulus function as well as the constant micromodulus function have jump discontinuities at $x=\pm\delta$ which lead to discontinuities in derivatives of the displacements [38] away from the point of application of the load. These discontinuities are proportional to the horizon size. In the numerical approximation the number of nodes inside the horizon will influence the results as well. For the double concentrated forces applied bar, assuming that the Nth derivative of the displacement u has a discontinuity at exactly one point x^*, the following equation relating jump discontinuities holds for any x (see [38]):

$$P[u^{(N+L+1)}]_x=[C^{(L)}]_{(x-x^*)}[u^{(N)}]_{x^*}+[b^{(N+L+1)}]_x \tag{28}$$

where N and L are the ranks of derivatives, $[\cdot]$ represent jump discontinuities in the corresponding function, and $P=6E/\delta^2$.

Using Equation (28) for $L=0$, $N=-2$, and $x=x^*=a$ gives

$$[u^{(-1)}]_a=\frac{\delta^2}{6E} \tag{29}$$

and then for $L=0$, $N=-1$, and $x=x^*=a$ gives

$$P[u^{(0)}]_a=[C^{(0)}]_0[u^{(-1)}]_a+[b^{(0)}]_a \tag{30}$$

$$[u^{(0)}]_a=\frac{\delta^2}{6E}[b^{(0)}]_a \tag{31}$$

Copyright © 2008 John Wiley & Sons, Ltd.

DOI: 10.1002/nme

The jumps at other locations away from the loading points are, for example:

$$[u^{(0)}]_{\delta-a} = [C^{(0)}]_{\delta}[u^{(-1)}]_{-a} = \frac{\delta}{12E} \tag{32}$$

$$[u^{(0)}]_{\delta+a} = [C^{(0)}]_{\delta}[u^{(-1)}]_{a} = \frac{-\delta}{12E} \tag{33}$$

Here $[u^{(-1)}]_{-a} = -[u^{(-1)}]_a$. Thus, analytically, the displacement field u has the same smoothness as the loading b in the peridynamic equations.

Numerically, for the point-load applied at a we have $[b^{(0)}]_a = b_0/\Delta x$, with $\delta = m\Delta x$. Here b_0 is the magnitude of the applied load at a, and Δx is the grid spacing (or the 'volume' of the node at a). Thus, in the numerical approximation $\tilde{u}$ we have the jump

$$[\tilde{u}^{(0)}]_a \sim \delta m \tag{34}$$

The following conclusions can be drawn about the behavior of the numerical solution for this problem:

(i) If δ is fixed and $m \to \infty$ (m-convergence), the singularity in the analytical peridynamic solution at a is obtained numerically, as well as the finite jump discontinuities at $\delta - a$ and $\delta + a$.
(ii) If $\delta \searrow 0$ and $m \nearrow \infty$, with m increasing faster than δ decreasing (the δm-convergence), the numerical approximation converges everywhere to the classical (local) solution and, at the points of application of singular loads, it converges to the analytical peridynamic, non-local, solution.
(iii) If $\delta \searrow 0$ and m is constant or increases but with $\lim_{m\to\infty,\delta\to 0} \delta m < \infty$ (the δ-convergence) the singularity at the loading point is approximated numerically by a finite jump discontinuity. If m is kept constant, the discontinuity is erased in the limit of δ going to zero (see Equation (34)). The approximation converges to the classical solution elsewhere.

4. ADAPTIVITY FOR PERIDYNAMICS

In peridynamics, adaptivity involves changes in the grid density as well as changes in the nodal horizons. These changes require, in turn, appropriate changes in the micromodulus function. In peridynamics, the process of changing the micromodulus when horizons change is called *scaling* [45].

4.1. Scaling and adaptivity in peridynamics

Assume a 1D bar like the one discussed above with two self-equilibrated concentrated loads but of finite length. The exact classical solution has constant strain between the points and zero elsewhere. For examples in 2D with stress/strain concentrations see [43].

There are two types of grid refinement: uniform and non-uniform refinement. In uniform refinement we solve the problem using uniform but denser and denser grids, while for non-uniform, selected regions are refined while other are not (see Figure 3). Note that in peridynamics, if we increase the density of the nodes then we deal with the m-type convergence. Because here we are trying to compare peridynamics with the classical, local, elasticity solutions, the goal is

Copyright © 2008 John Wiley & Sons, Ltd.

DOI: 10.1002/nme

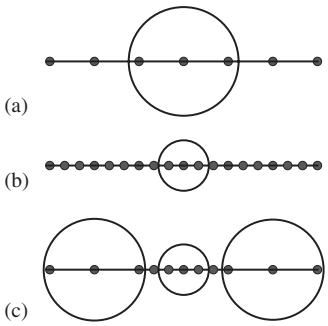

Figure 3. Schematic plot of refinement: uniform refinement between (a) and (b), and non-uniform refinement in (c) based on scaling.

the (δm)-type convergence, where the horizon goes to zero. In adaptive refinement, the change of horizon has to be done only in regions of interest, outside which the horizon (and thus the discretization size) can stay large to save computational resources. Some examples of requirements for the horizon size needed to resolve wave propagation in a 1D bar with an insignificant amount of dispersion are given in [41].

Assume that using two different horizons, δ and ε, we want the material models corresponding to these horizons to be equivalent in the sense that under a given homogeneous deformation, the strain energy is the same in the two regions corresponding to the two horizons (see Figure 3). In order to correctly perform this mixed description of a material using two different horizons, scaling is necessary. Scaling in 3D is derived in [45] by requiring the following change in the micropotential (thus micromodulus) function:

$$w_\varepsilon(\eta, \xi) = \gamma^3 w_\delta(\gamma\eta, \gamma\xi) \tag{35}$$

where $\gamma = \delta/\varepsilon$ is the geometrical scaling of the horizon size. The 1D version of this scaling is

$$w_\varepsilon(\eta, \xi) = \gamma w_\delta(\gamma\eta, \gamma\xi) \tag{36}$$

It is easy to confirm that this scaling relation for the micropotential indeed results in the same strain energy density at a point x in the bar

$$\bar{W}_\delta(x) = \frac{A}{2}\int_{H_\delta} w_\delta(\gamma\eta, \gamma\xi)\,\mathrm{d}(\gamma\xi) = \frac{A}{2}\int_{H_\varepsilon} \frac{1}{\gamma} w_\varepsilon(\eta, \xi)\gamma\,\mathrm{d}\xi = \bar{W}_\varepsilon(x) \tag{37}$$

4.2. Implementing scaling and adaptivity in peridynamics

To perform grid adaptivity, we need to employ scaling as shown in Figure 3(c). Assume we have a region U and a refined region R where the node horizon is smaller and the node discretization is denser. If the horizon of a node in region U does not cover any node (or part of its volume) from region R, and vice versa, then the micromodulus of the node is that computed from, for example, (15) or (16) or (19). Determining the micromodulus for the rest of the nodes needs to be addressed. We propose the following natural strategy: assume that node i in region U (with a horizon ε) 'covers' a node j in region R (with a horizon δ). The micromodulus of the bond connecting the 'source' node i to the 'field' node j is that corresponding to the horizon of the

Copyright © 2008 John Wiley & Sons, Ltd.

DOI: 10.1002/nme

'source' node i. The same strategy is employed when the roles of regions U and R are exchanged. Thus, our strategy for scaling obeys the rule that all bonds inside the horizon of the 'source' node have the micromodulus corresponding to the 'source' node horizon.

We now show that this scheme satisfies Newton's third law in the 'overlap' region between two different horizons. Indeed, for a source point x in the region with small horizons, δ, the micropotential is given by

$$w(\eta, \xi, x) = \frac{c(\xi, \delta)s^2|\xi|}{2} \tag{38}$$

Using the proposed method, the micropotential of the point at $x+\xi$, irrespective of whether this point belongs to the U or R regions, will be

$$w(-\eta, -\xi, x+\xi) = \frac{c(-\xi, \delta)s^2|\xi|}{2} = \frac{c(\xi, \delta)s^2|\xi|}{2} \tag{39}$$

with the last equality due to the requirement that the micromodulus function be even (see, e.g. [38, 39]). The force density at x is then

$$f(\eta, \xi, x) = \frac{\partial w(\eta, \xi, x)}{\partial \eta} = c(\xi, \delta)s\frac{|\xi|}{|\xi|} = c(\xi, \delta)s \tag{40}$$

while the force at $x+\xi$ is

$$f(-\eta, -\xi, x+\xi) = \frac{\partial w(-\eta, -\xi, x+\xi)}{\partial \eta} = -c(\xi, \delta)s = -f(\eta, \xi, x) \tag{41}$$

The method proposed here is a first step toward developing multiscale methods in peridynamics. In the following sections we implement and test this method for static and dynamic elasticity problems in 1D.

5. ADAPTIVITY FOR STATIC ELASTICITY PROBLEMS

To demonstrate adaptivity in static problems, we consider the 1D bar with the two self-equilibrated forces applied at some a and $-a$. We take $E=1$. From Section 2.2, we know that $u_\infty = a$. We choose an error estimator based on a point-wise value: the relative error for the displacement field at some point between a and $-a$. This is similar to what is used in the so-called goal-oriented adaptive refinement methods. Error estimators based on global measures (using the 2-norm) can also be used, and have been used with identical results.

5.1. Influence of the placement of the refinement region with respect to the loaded region

We first analyze the sensitivity of the solution to the placement of the refinement region with respect to the two concentrated loads. For this, we consider $a=1$ and the total length of the bar to be 4 units, thus the ends of the bar are at -2 and 2. We define fours cases (see Figure 4):

Case (a): The refinement zone contains the interval $[-a, a]$; however, there still are nodes in the unrefined region that cover, with their horizons, the locations where the concentrated loads are applied.

Copyright © 2008 John Wiley & Sons, Ltd.

DOI: 10.1002/nme

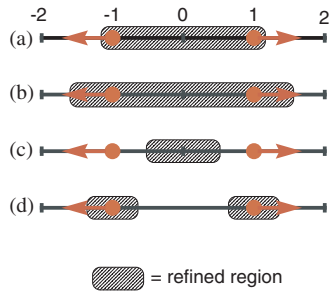

Figure 4. The four cases for the placement of the refinement region with respect to the position of the loaded zone.

Case (*b*): Same as (a) but the refined region extends sufficiently outside $[-a, a]$ so that the points of application of the loads are not 'seen' by any of the nodes in the unrefined regions. The points where the loads are applied are covered only by horizons of nodes in the refined region.

Case (*c*): A region completely inside $[-a, a]$ is refined.

Case (*d*): The refined areas regions cover the loading points and the nodes in the unrefined region do not cover a and $-a$ with their horizons.

The refinement strategy we implement is one that increases the node density by the same factor with which we decrease the horizon. Thus, in regions away from transition zones, where the node density and the horizon size are constant, the number of nodes inside a horizon is constant. In the transition zone between refined and unrefined grids, several choices can be made: a sudden change from large node volume/horizon to the smaller volume/horizon, a gradual transition, or a step-wise transition. The differences between these appear to be small. In what follows, we present the results from the sudden change in grid density.

We first compare the above four cases and the effect of using the constant (discontinuous) and the triangular (continuous) micromodulus function (see Figure 1). The comparisons are with the classical analytical solution in (23) at point $x = 0.5$. The results for the convergence rates measured using norm-2 show exactly the same trends.

The rates of convergence for non-uniform grids, obtained via linear curve fit of the data in Table I, are 1.175, 1.179, 1.165, and 1.355, respectively, for constant micromodulus. The rates of convergence are 1.800, 2.040, 1.745, and 1.860, respectively, for triangle micromodulus. The details for these results are given in Table I. We conclude that

1. The convergence rate in the non-uniform refinement solution is better when a continuous micromodulus function is used compared with a discontinuous micromodulus (see Figure 5).
2. The maximum convergence rates and the smallest errors are obtained in cases when the loaded zones are covered by refined nodes only (cases b and d) compared with all other cases. The following '*visibility criterion*' should, therefore, be used: *if a refined solution is sought at a point x, then the nodes in the coarse region should not cover* (*or* '*see*') *with their horizons the point x.*

5.2. *Comparison between uniform and non-uniform refinement*

The example we analyze does not have a strain concentration region; except for the loading points, the strain is constant in the limit of horizon going to zero. The same is true for the classical

Copyright © 2008 John Wiley & Sons, Ltd.

DOI: 10.1002/nme

Table I. Influence of the placement of the refinement region with respect to the loaded region for continuous and discontinuous micromodulus functions.

	Number of nodes inside horizon, m	Horizon size	Total number of nodes	Relative error (%)
Case (a)	22.8–22.6	0.200–0.450	201	0.903
and constant	34.0–33.6	0.150–0.320	401	0.378
micromodulus	44.8–43.0	0.133–0.280	601	0.253
	56.0–55.8	0.125–0.265	801	0.175
Case (a)	23.4–23.8	0.200–0.440	201	1.003
and triangular	33.0–33.2	0.150–0.310	401	0.309
micromodulus	43.8–43.0	0.133–0.275	601	0.158
	55.0–54.7	0.125–0.260	801	0.079
Case (b)	23.8–24.2	0.200–0.440	201	0.428
and constant	33.0–33.5	0.150–0.310	401	0.159
micromodulus	43.2–42.9	0.133–0.275	601	0.123
	55.2–54.8	0.125–0.260	801	0.079
Case (b)	23.4–23.8	0.200–0.440	201	0.380
and triangular	33.0–33.2	0.150–0.310	401	0.072
micromodulus	43.8–43.0	0.133–0.275	601	0.047
	55.0–54.7	0.125–0.260	801	0.020
Case (c)	22.3–22.2	0.200–0.440	201	3.524
and constant	32.1–32.5	0.150–0.310	401	1.372
micromodulus	42.5–42.6	0.133–0.275	601	0.972
	54.3–52.8	0.125–0.260	801	0.692
Case (c)	23.4–23.8	0.200–0.440	201	2.412
and triangular	33.0–33.2	0.150–0.310	401	0.631
micromodulus	43.8–43.0	0.133–0.275	601	0.398
	55.0–54.7	0.125–0.260	801	0.199
Case (d)*	23.2–23.5	0.200–0.410	201	0.618
and constant	33.0–33.3	0.150–0.320	401	0.172
micromodulus	43.5–43.1	0.133–0.260	601	0.134
	55.2–54.9	0.125–0.230	801	0.092
Case (d)	23.4–23.8	0.200–0.410	201	0.562
and triangular	33.0–33.2	0.150–0.310	401	0.126
micromodulus	43.8–43.0	0.133–0.275	601	0.079
	55.0–54.7	0.125–0.260	801	0.040

*For case d, we measure the displacement at point $x = 0.7$ in order to fall inside the refined region.

solution. Thus, when adaptive refinement is used in this case we expect convergence rates of the non-uniformly refined solution to be the same as those obtained using uniform grid refinement (see also, [18]).

We compare the uniform versus non-uniform refinement for the same bar as before but now extended to a length of 20 units so that the refinement zone in the non-uniform refinement case is a small fraction (below 15%) of the total bar length, a likely scenario in practice. Using the same number of nodes and selecting case b (in which the loaded area is covered only by refined nodes)

Copyright © 2008 John Wiley & Sons, Ltd.

DOI: 10.1002/nme

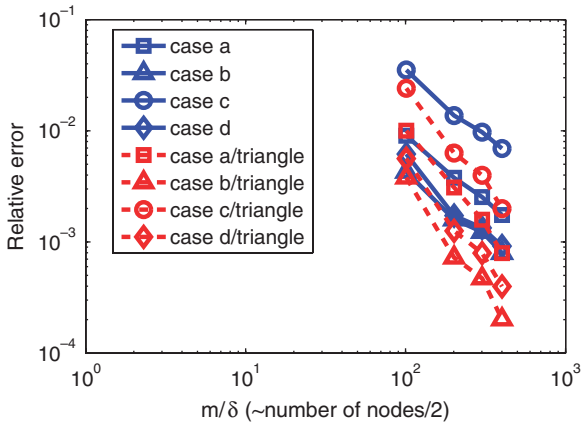

Figure 5. Convergence rates for the static problem for different placements of the refinement region, and using continuous (triangular) and discontinuous (constant) micromodulus functions.

Table II. Comparison between uniform and non-uniform (or adaptive) double and quadruple refinement for the static problem. Relative errors from the classical analytical solution.

		Uniform refinement		Double refinement		Quadruple refinement	
Total number of nodes	Number of nodes in horizon	Constant micromod. (%)	Triangular micromod. (%)	Constant micromod. (%)	Triangular micromod. (%)	Constant micromod. (%)	Triangular micromod. (%)
201	21(23–24)*	3.375	3.745	1.172	1.047	0.627	0.562
401	31(32–33)	1.025	1.259	0.625	0.331	0.285	0.178
601	41(42–45)	0.516	0.562	0.454	0.170	0.200	0.101
801	51(54–56)	0.259	0.288	0.314	0.109	0.139	0.055

*The numbers in parenthesis are for the non-uniform refinement cases (the number of nodes inside horizon is kept as constant as possible along the bar).

above, the non-uniform refinement solution reduces the relative error and saves computational time compared with the uniform refinement solution. This is seen from Table II and Figure 6, where we use uniform and non-uniform refinement for constant and triangular micromodulus functions. For the non-uniform refinement we also compute the solution by changing the density of nodes between the refined and non-refined regions by two times (and halving the horizons) and four times (and reducing the horizon size four times).

The results in Table II and in Figure 6 show that the rate of convergence for uniform refinement is 1.822 and 1.834 for constant micromodulus and triangle micromodulus, respectively. The rate of convergence for non-uniform refinement with 2-times refinement and 4-times refinement is 0.9296 and 1.0722 for constant micromodulus and 1.643 and 1.642 for triangle micromodulus, respectively. The rate reaches 2.058 for the quadruple refinement with triangular micromodulus between the last two data points.

Non-uniform refinement improves the relative error in the solution greatly compared with the uniform solution using the same number of nodes in the bar. Increasing the refinement level (from

Copyright © 2008 John Wiley & Sons, Ltd.

DOI: 10.1002/nme

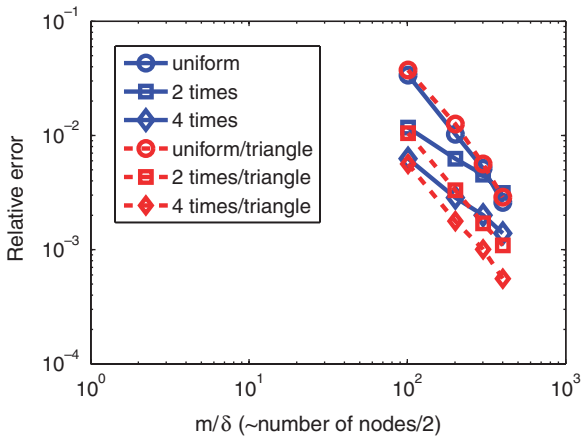

Figure 6. Comparison between uniform and non-uniform refinement. For non-uniform refinement, different levels (double, quadruple) are tested.

2 to 4) also increases the solution accuracy, independent of the form of the micromodulus function. As expected from the results in the previous section, the continuous micromodulus (triangular) leads to higher convergence rates and considerably smaller relative errors than a discontinuous (constant) micromodulus function.

We conclude that

1. The rate of convergence for *uniform* grids is not sensitive to the specific shape or smoothness of the micromodulus function.
2. For the non-uniform grids used in adaptive refinement, the strong cut-off in micromodulus at the boundary of its horizon (discontinuous micromodulus) lowers the rate of convergence from quadratic to super-linear (see Figure 6). The reason for this behavior is a subject of further study.

6. ADAPTIVITY FOR ELASTO-DYNAMIC PROBLEMS IN PERIDYNAMICS

Based on the scaling theory discussed in Section 4, a 1D example is examined for wave propagation on uniform and non-uniform grids. Here, we analyze a Gaussian wave propagating along a 1D bar with free ends. The propagation of discontinuous waves in peridynamics is studied in [41, 42]. The length of the bar is $L=300$, cross-section area $A=1$, and Young's modulus $E=1$. The initial displacement imposed on the elastic bar is a half Gaussian of the form $u(x)=0.02\mathrm{e}^{-0.01x^2}$, and is shown in Figure 7. For the time integration we use the Runge–Kutta method while for the spatial integration the midpoint rule is used.

6.1. Error estimators and grid refinement algorithm

For the dynamic problem we use error estimators based on the wave speed (related to the conservation of kinetic energy) and compute the arrival time of the peak of the wave at some prescribed

Copyright © 2008 John Wiley & Sons, Ltd.

DOI: 10.1002/nme

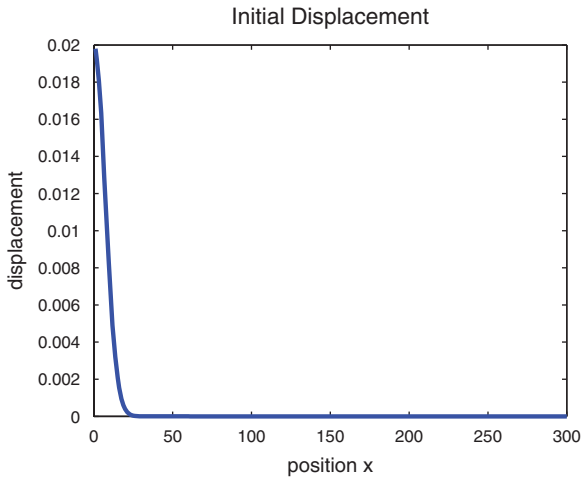

Figure 7. Initial displacement along the bar.

location along the bar, and the wave amplitude (related to the potential strain energy conservation) at the same location and at the same time.

For a Gaussian displacement of the form $u(x) = a\mathrm{e}^{-\omega x^2}$, the strain energy equals $\sqrt{(\pi\omega/2)}Ea^2/2$, where a is the amplitude of the full Gauss wave. The kinetic energy is proportional to $\rho v^2/2$, where v is the wave's velocity. We define the relative error between the exact and the numerical wave amplitude, and the exact and numerical times-of-arrival at the midpoint as follows:

$$\frac{|A_{\mathrm{ex}} - A_{\mathrm{num}}|}{A_{\mathrm{ex}}} \quad \text{and} \quad \frac{|T_{\mathrm{ex}} - T_{\mathrm{num}}|}{T_{\mathrm{ex}}}$$

The total energy (kinetic plus potential) is used as the adaptive triggering mechanism. At every time step we compute the maximum and the minimum total energy among all nodes. Points where the energy is less than a certain threshold value (close to the maximum value) are not refined (or are coarsened, if they have been refined before). Nodes where the energy is larger than the same threshold are refined. Through this process, the refined grid together with the scaled horizons and micromoduli move together with the wave.

Note, again, that adaptive refinement in peridynamics involves not only the increase in node density (the classical h-refinement), but also changing the horizon and micromodulus function. If we only refine the spatial grid, that leads to m-convergence (see Section 3.1). The algorithm used in the adaptive refinement for the dynamic case is given in Algorithm 1.

6.2. Examples and numerical results

6.2.1. Effect of non-uniform numerical integration. We first analyze the effect of changing the density of nodes (the size of the integrating nodal volume Δx) on the propagation of a smooth wave while keeping the horizon constant along the bar. The node density is increased in the middle third part of the bar with the horizons (and therefore the micromoduli) kept the same. In effect, we use a more accurate numerical integration of the force integral in Equation (1) in the middle third of the beam than outside it and monitor the effect on the reflection of the wave from this. Note

Copyright © 2008 John Wiley & Sons, Ltd.

DOI: 10.1002/nme

Algorithm 1 Adaptive refinement for peridynamics: 1D dynamic wave propagation

```
input initial data
initialize node refinement level with 1.
select nodes above threshold energy density value; classify nodes into: to be refined, to be
  coarsened, and unchanged.
for all nodes in to be refined region do
   generate additional nodes between current node and its neighboring nodes.
   interpolate displacement, velocity and acceleration, density, etc. to the new node.
   update volume and horizon of the new node.
end for nodes in to be refined region
for all nodes in to be coarsened region do
   if the refinement level of the node is equal to 1 then
      continue
   else
      delete node;
   end if
end for nodes in to be coarsened region
```

that this is not 'refinement' in the sense introduced before, where the horizon and micromodulus are changed by scaling. In these simulations we use a horizon size that is sufficiently small so that the dispersion due to the horizon size is not noticeable (see also, [41, 42]). We test two cases of increasing node density at the middle third of the bar:

Case (*a*): Doubling of node density: there are 1000 nodes in the middle third part and a total of 2000 along the entire bar.

Case (*b*): Quadrupling of node density: there are 2000 nodes in the middle section and a total of 3000 along the entire bar; therefore, the node density in the central region is four times that outside it.

From the results shown in Figure 8, the non-uniform grids introduce, as expected, reflection waves from the interfaces of different grids. Two different micromodulus functions, constant (Figure 8(a)) and triangular (Figure 8(b)), are used and the reflected peak wave arrival time and amplitude are measured at the midpoint of the bar. The analytical arrival time is 250.

From Table III we observe that using the triangular micromodulus (a particular type of continuous micromodulus) significantly reduces the amplitude of the reflected wave (by more than 50% compared with the discontinuous micromodulus). The arrival time at the midpoint is also improved when using triangle micromodulus function when the jump in grid density is only double in the region with finer integration (higher nodal density). As expected, the larger the difference between the node density over different parts of the bar, the larger the amplitude of the reflection waves. This is simply due to the change in numerical integration accuracy. How to completely eliminate this numerical reflection is not clear at this point and is subject to further study.

Using a large number of nodes inside the horizon (m) and small horizons (relative to the wavelength of the propagating wave) reduces the numerical dispersion due to numerical discretization. This type of numerical dispersion is seen in classical methods approximating the classical continuum mechanics equations, and in fact in any discretization method. A discussion of these aspects related to classical methods is given in [7].

Copyright © 2008 John Wiley & Sons, Ltd.

DOI: 10.1002/nme

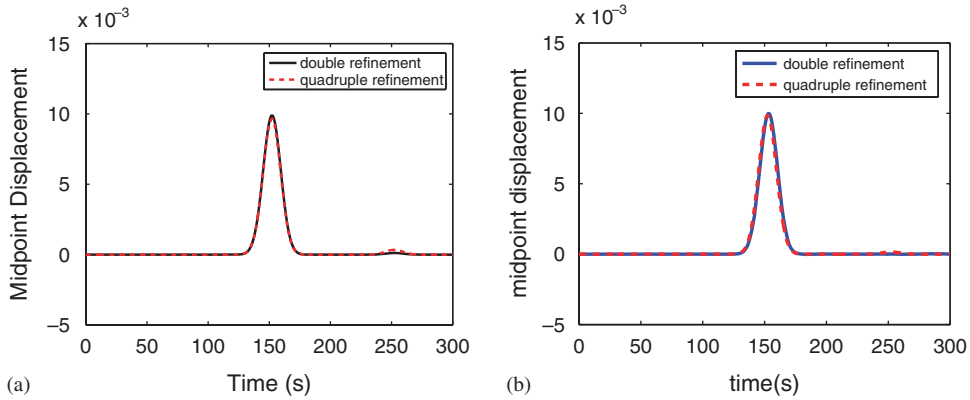

Figure 8. Effect of non-uniform grids on wave propagation in 1D peridynamic materials for the case of non-varying horizon and micromodulus: (a) effect of using non-uniform integration and constant discontinuous and (b) continuous micromodulus with a constant horizon of 0.5.

Table III. Influence of micromodulus continuity and abrupt change in node-density or spatial integration (horizon is kept constant along the bar) on the propagating wave. Relative errors from the classical analytical solution.

	Type of micromodulus function	Arrival time at midpoint	Amplitude at midpoint ($\times 10^{-4}$)	Relative error for arrival time (%)	Reflected wave amplitude as portion of main wave amplitude (%)
Case (a)	Constant	252.15	1.169	0.86	1.169
	Triangle	249.15	0.0844	0.34	0.084
Case (b)	Constant	252.30	3.3557	0.92	3.356
	Triangle	252.30	1.4945	0.92	1.495

Figure 8 shows that if the integration accuracy is abruptly changed in the domain, a small portion of the wave energy is reflected when the wave passes through the boundary between the denser integrating region. The reflection is smaller for a continuous micromodulus compared with a discontinuous micromodulus. As expected, the larger the jump in integration accuracy the larger the reflection. However, even when the integration nodal density changes by a factor of four, the amount of the reflected energy is insignificant compared with the total energy of the wave.

6.2.2. Uniform and adaptive refinement for wave propagation in 1D. We now turn to using the scaling theory discussed in Section 4 and Algorithm 1 to implement adaptive non-uniform refinement and coarsening for wave propagation in a 1D bar. We compare two cases using the triangular micromodulus function since, as we have seen in the static case, the continuous micromodulus function maintains the rate of convergence even when non-uniform grids are used in refinement:

Case a: Uniform refinement.

Case b: Non-uniform refinement and coarsening. Adaptive refinement is triggered when the energy at a node is at least 75% of the largest total energy among all nodes. In addition, all nodes

Copyright © 2008 John Wiley & Sons, Ltd.

DOI: 10.1002/nme

Table IV. Convergence for uniform refinement (Case a) for the wave propagation example. Relative errors from the classical analytical solution.

Nodes inside horizon	Total nodes number	Horizon size	Arrival time of wave peak at coord. $x=400$	Amplitude of peak wave at coord. $x=400$	Relative error for arrival time (%)	Relative error amplitude (%)
7	451	3.0	426.60	0.00970	6.65	2.93
11	901	2.5	409.95	0.00982	2.49	1.77
13	1351	2.0	406.80	0.00991	1.70	0.84
21	2701	1.5	403.20	0.00997	0.80	0.30
23	3001	1.4	402.15	0.00998	0.53	0.23

Table V. Convergence for adaptive refinement with refinement threshold at 75% of the maximum nodal energy (Case b) for the wave propagation example. Relative errors from the classical analytical solution.

Nodes inside horizon	Total nodes number	Horizon size	Arrival time of wave peak at coord. $x=400$	Amplitude of peak wave at coord. $x=400$	Relative error for arrival time (%)	Relative error for amplitude (%)
7	451	3.0	415.35	0.00987	3.83	1.24
(7–11)*	(487–517)	(1.5–3.0)				
11	901	2.5	405.90	0.00991	1.47	0.84
(11–13)	(966–1018)	(1.25–2.5)				
13	1351	2.0	403.95	0.00996	0.98	0.38
(13–16)	(1438–1507)	(1.0–2.0)				
21	2701	1.5	401.85	0.00999	0.46	0.11
(21–24)	(2857–2975)	(0.75–1.5)				
22	2801	1.5	401.40	0.01000	0.35	0.09
(22–25)	(2959–3081)	(0.71–1.4)				

*Numbers in parenthesis represent the range of values during refinement.

within a length equal to six-times the size of the largest horizon in the grid from the node to be refined are also refined.

In order to have the refinement region represent a small part (less than 20%) of the total length, we now choose $L=450$ and we measure the time of arrival of the peak of the wave at $x=400$. The amplitude of the peak is measured at the same time. Using the same setup for the 1D bar as listed in the beginning of Section 6, the wave propagation in the peridynamic bar is analyzed and the results are summarized in Tables IV and V. These results lead to the following rates of convergence: the uniform refinement reaches a rate of 1.245 for the arrival time of the peak wave and 1.371 for the peak amplitude at that time; the rates of convergence of the adaptive refinement method is 1.234 for the arrival time and 1.492 for the peak amplitude. In Figure 9, for the adaptive refinement case, we choose the average number of nodes used in the refinement process for the values along the x-axis. We observe uniform convergence for both uniform and non-uniform (adaptive) refinement in smooth wave propagation along a 1D bar with peridynamics. The relative error for the adaptive refinement is below the one obtained with uniform refinement and, the smaller the adaptively refined zone, relative to the total length traveled by the wave, the better the adaptive solution becomes, relative to the uniformly refined solution. The convergence rate to the classical solution

Copyright © 2008 John Wiley & Sons, Ltd.

DOI: 10.1002/nme

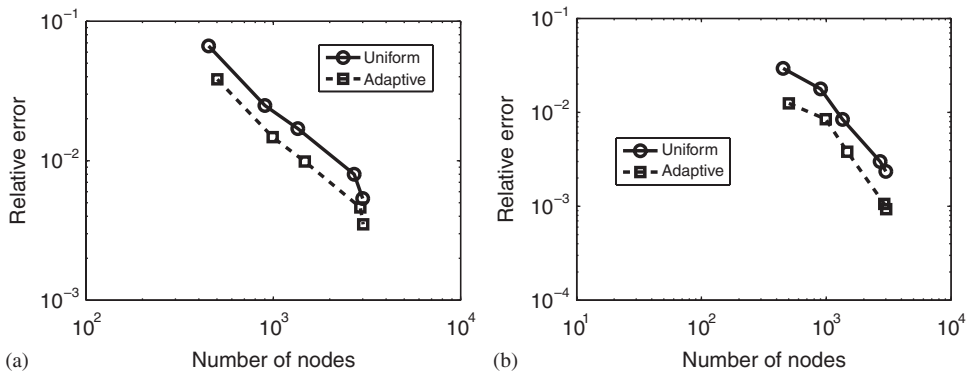

Figure 9. Uniform and adaptive refinement rates of convergence for smooth wave propagation in a 1D bar: (a) convergence rates for the peak wave arrival time at $x = 400$ along the bar and (b) wave peak amplitude. Relative errors from the classical analytical solution.

increases as more nodes are used because the horizon size also decreases (due to scaling) and this leads to a significant decrease in wave dispersion (see also [41, 42]).

We should mention that in contrast with the classical continuum formulation in one dimension, the corresponding 1D peridynamic formulation does introduce horizon-related dispersion in addition to the numerical dispersion (see also [39]). In higher dimensions, the classical continuum formulation also exhibits physical dispersion. A strict distinction between the dispersion due to the numerical approximation and that due to the formulation is not always possible. In peridynamics, using a continuous micromodulus instead of a discontinuous micromodulus function reduces horizon-related dispersion significantly and improves the rate of convergence, as shown above for both the static and dynamic cases. We also note that propagation of discontinuous waves (such as shock waves) requires special treatment. This topic is analyzed in [41, 42].

With a discontinuous micromodulus we do not obtain uniform convergence to the classical results for the dynamic case.

7. CONCLUDING REMARKS

The peridynamic model is non-local and contains a length-scale determined by the horizon δ. In some problems, particularly at the nanoscale, the horizon is determined by the physics of interactions between particles. However, at the macroscale level, the horizon may be chosen according to convenience, since for any value of δ, the parameters in the peridynamic material model can be chosen to match the measured Young's modulus of the material. To allow large variations in grid spacing within a discretized region, needed in grid refinement and multiscale modeling, one has to allow the horizon to vary with position.

In this paper, we introduced, for the first time, adaptive refinement for the non-local peridynamics method. Adaptive refinement in peridynamics requires scaling of the nodal horizons and micromoduli. We clarified various types of convergence in peridynamics that allow comparisons with the classical, local elasticity solutions. We obtained uniform convergence toward the classical solutions of static and dynamic elasticity problems in 1D. The match of the horizon and

Copyright © 2008 John Wiley & Sons, Ltd.

DOI: 10.1002/nme

micromodulus function to the elastic modulus has been set for the case of homogeneous deformations. Our results showed, however, that even for non-homogenous deformations the approach is valid and that it leads to convergence to the classical, local elasticity solutions.

The effect of different micromodulus functions has also been discussed. We found that using discontinuous micromodulus functions (functions with jump discontinuity at the edge of the horizon) reduces the quadratic rate of convergence to linear or super-linear, for non-uniform refinement. Interestingly, the optimal rate of convergence is preserved for uniform refinement with a discontinuous micromodulus function. Continuous micromoduli showed quadratic convergence independent of the refinement type. Solutions obtained on uniform grids did not appear to be sensitive to the micromodulus shape, in the limit of horizon going to zero. As a refinement strategy, the '*visibility criterion*' should be used: if a refined solution is sought at a point x, then the nodes in the coarse regions should not cover (or 'see') the points x with their horizons.

Moreover, we showed that the use of 'exotic' micromoduli (inverted triangular), while valid from the point of view of material stability, can lead to ill-conditioning of the stiffness matrix for static problems. Even in these cases, however, a correct solution is possible using dynamic relaxation instead of building the stiffness matrix. The examples we gave from elasto-static and elasto-dynamic analyses in 1D, showed that the adaptive peridynamic solution achieves the same (or very similar) rates of convergence as uniform refinement, which is expected for problems where there are no strain concentrations. Notably, the relative error for the solutions obtained using adaptive refinement are significantly lower than those obtained using uniform refinement with the same number of nodes. The advantage of adaptive refinement becomes critical in problems where small, localized regions feature strain and stress concentrations, like regions around crack tips. The methods introduced in this paper are extended to 2D and used for problems with strain localization and crack propagation in [43].

ACKNOWLEDGEMENTS

The work of the first three authors has been supported by funds from the Boeing Co. via a sub-contract from Sandia National Labs awarded to the University of Nebraska-Lincoln. Sandia is a multiprogram laboratory operated by Sandia Corporation, a Lockheed Martin Company, for the United States Department of Energy's National Nuclear Security Administration under contract DE-AC04-94AL85000. This work was partially supported by the Computer Science Research Foundation and Computer Science Research Institute at Sandia National Laboratories.

REFERENCES

1. Babuska I, Rheinboldt WC. A posteriori error estimates for the finite element method. *International Journal for Numerical Methods in Engineering* 1978; **1**(12):1597–1615.
2. Zienkiewicz OC, Zhu JZ. A simple error estimator and adaptive procedure for practical engineering analysis. *International Journal for Numerical Methods in Engineering* 1987; **24**(2):337–357.
3. Rachowicz W, Oden JT, Demkowicz L. Toward a universal *hp*-adaptive finite element strategy. Part 3: design of *hp* meshes. *Computer Methods in Applied Mechanics and Engineering* 1989; **77**:181–212.
4. Demkowicz L, Oden JT. Application of *hp*-adaptive be/fe methods to elastic scattering. *Computer Methods in Applied Mechanics and Engineering* 1996; **133**:287–318.
5. Oden JT, Prudhomme S. Goal-oriented error estimation and adaptivity for the finite element method. *Computers and Mathematics with Applications* 2001; **41**(5–6):735–756.
6. Rachowicz W, Pardo D, Demkowicz L. Fully automatic hp-adaptivity in three dimensions. *Computer Methods in Applied Mechanics and Engineering* 2006; **195**(37–40):4816–4842.

Copyright © 2008 John Wiley & Sons, Ltd.

DOI: 10.1002/nme

7. Bazant Z. Spurious reflection of elastic waves in nonuniform finite element grids. *Computational Methods in Applied Mechanics and Engineering* 1978; **16**:91–100.
8. Celep Z, Bazant Z. Spurious reflection of elastic waves due to gradually changing finite element size. *International Journal for Numerical Methods in Engineering* 1983; **19**:631–646.
9. Zienkiewicz OC, Xie Y. A simple local error estimate and an adaptive time-stepping procedure for dynamic analysis. *Earthquake Engineering and Structural Dynamics* 1991; **22**:871–887.
10. Cavin P, Gravouil A, Lubrecht AA, Combescure A. Automatica energy conserving space–time refinement for linear dynamic structural problems. *International Journal for Numerical Methods in Engineering* 2005; **64**:304–321.
11. Schweizerhof K, Neumann J, Riccius J. Adaptive analysis of plate and shell structures under transient loading. In *Error-Controlled Adaptive Finite Elements in Solid Mechanics*, Stein E (ed.). Wiley: New York, 2002; 309–345.
12. Bangert W, Rannacher R. Finite element approximation of the acoustic wave equation: error control and mesh adaption. *East-West Journal of Numerical Mathematics* 1999; **7**(4):263–282.
13. Kanschat G. Multilevel methods for discontinuous Garlerkin fem on locally refined meshes. *Computers and Structures* 2004; **82**:2437–2445.
14. van Dommelen L, Rundensteiner EA. Adaptive summation of point forces in the two-dimensional poisson equation. *Journal of Computational Physics* 1989; **83**:126–147.
15. De Zeeuw D, Powell KG. An adaptively rened cartesian mesh solver for the euler equations. *Journal of Computational Physics* 1993; **104**:56–68.
16. Becker R, Johnson C, Rannacher R. Adaptive error control for multigrid finite element methods. *Computing* 1995; **55**:271–288.
17. Tabarraei A, Sukumar N. Adaptive computations on conforming quadtree meshes. *Finite Elements in Analysis and Design* 2005; **41**:686–702.
18. Rabczuk T, Belytschko T. Adaptivity for structured meshfree particle methods in 2d and 3d. *International Journal for Numerical Methods in Engineering* 2005; **63**(11):1559–1582.
19. Bazant ZP, Jirasek M. Nonlocal integral formulations of plasticity and damage: survey of progress. *Journal of Engineering Mechanics* 2002; **128**(11):1119–1149.
20. Rodriguez-Ferran A, Huerta A. Error estimation and adaptivity for nonlocal damage models. *International Journal of Solids and Structures* 2000; **37**(48–50):7501–7528.
21. Comi C, Perego U. Criteria for mesh refinement in nonlocal damage finite element analyses. *European Journal of Mechanics A-Solids* 2004; **23**(4):615–632.
22. Rodriguez-Ferran A, Morata I, Huerta A. Efficient and reliable nonlocal damage models. *Computer Methods in Applied Mechanics and Engineering* 2004; **193**(30–32):3431–3455.
23. Patzak B, Jirasek M. Adaptive resolution of localized damage in quasi-brittle materials. *Journal of Engineering Mechanics—ASCE* 2004; **130**(6):720–732.
24. Silling SA. Reformulation of elasticity theory for discontinuities and long-range forces. *Journal of the Mechanics and Physics of Solids* 2000; **48**:175–209.
25. Silling SA, Askari E. A meshfree method based on the peridynamic model of solid mechanics. *Computers and Structures* 2005; **83**(17–18):1526–1535.
26. Silling SA, Bobaru F. Peridynamic modeling of membranes and fibers. *International Journal of Non-Linear Mechanics* 2005; **40**:395–409.
27. Bobaru F. Influence of van der waals forces on increasing the strength and toughness in dynamic fracture of nanofiber networks: a peridynamic approach. *Modelling and Simulation in Materials Science and Engineering* 2007; **15**:397–417.
28. Eringen AC, Edelen DGB. On non-local elasticity. *International Journal of Engineering Science* 1972; **10**:233–248.
29. Eringen AC. Theory of nonlocal elasticity: some applications. *Research in Mechanics* 1987; **21**:313–342.
30. Kunin IA. *Elastic Media with Microstructure I*: *One-dimensional Models* (1st edn). Springer: Berlin, 1982.
31. Rogula D. *Nonlocal Theory of Material Media*. Springer: Berlin, 1982.
32. Bazant Z, Belytschko T, Cheng TP. Continuum theory for strain-softening. *Journal of Engineering Mechanics* 1984; **110**:1666–1692.
33. Bazant Z, Belytschko T. Wave propagation in a strain-softening bar: exact solution. *Journal of Engineering Mechanics* 1985; **111**(3):381–389.
34. Lehoucq RB, Silling SA. Force flux and the peridynamic stress tensor. *Journal of the Mechanics and Physics of Solids* 2008; **56**(4):1566–1577.
35. Askari E, Xu J, Silling SA. Peridynamic analysis of damage and failure in composites. *44th AIAA Aerospace Sciences Meeting and Exhibition*, number AIAA 2006-88, Reno, NV, January 2006.

Copyright © 2008 John Wiley & Sons, Ltd.

DOI: 10.1002/nme

36. Xu J, Askari A, Weckner O, Razi H, Silling SA. Damage and failure analysis of composite laminates under biaxial loads. *48th AIAA/ASME/ASCE/AHS/ASC Structures*, *Structural Dynamics*, *and Materials* (*SDM*) *Conference*, number AIAA 2007-2315, Honolulu, HI, April 2007.
37. Colavito KW, Kilic B, Celik E, Madenci E, Askari E, Silling SA. Effect of void content on stiffness and strength of composites by a peridynamic analysis and static indentation test. *48th AIAA/ASME/ASCE/AHS/ASC Structures*, *Structural Dynamics*, *and Materials* (*SDM*) *Conference*, number AIAA 2007-2251, Honolulu, HI, April 2007.
38. Silling SA, Zimmermann M, Abeyaratne R. Deformation of a peridynamic bar. *Journal of Elasticity* 2003; **73**(1–3):173–190.
39. Weckner O, Abeyaratne R. The effect of long-range forces on the dynamics of a bar. *Journal of the Mechanics and Physics of Solids* 2005; **53**(3):705–728.
40. Otter JRH. Computations for prestressed concrete reactor pressure vessels using dynamic relaxation. *Nuclear Structural Engineering* 1965; **1**(1):61–75.
41. Xie W. Peridynamic flux-corrected transport algorithm for shock wave studies. *Master's Thesis*, University of Nebraska-Lincoln, Department of Engineering Mechanics, Lincoln, NE, August 2005.
42. Bobaru F, Xie W. A flux-corrected transport peridynamic formulation for impact and spallation. 2008, submitted for publication.
43. Bobaru F, Yang M, Alves LF, Silling SA, Askari E. Adaptive refinement with peridynamics in 2d. 2008, submitted for publication.
44. Emmrich E, Kusche S, Büsing H. Numerical methods in the peridynamic theory: improved quadrature. *Technical Report*, Technical University of Berlin, Mathematics Institute, Berlin, Germany, October 2006.
45. Silling SA. Homogenization and scaling of peridynamic material models. *Unpublished Report*, July 2005.

Copyright © 2008 John Wiley & Sons, Ltd.

DOI: 10.1002/nme